Neuropharmacology 285 (2026) 110804

Contents lists available at ScienceDirect

Neuropharmacology

journal homepage: www.elsevier.com/locate/neuropharm

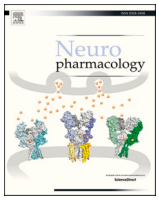

Assessment of the therapeutic effect of IGS2.7, a CK1δ protein kinase inhibitor, in combination with riluzole for the treatment of ALS-associated TDP-43 proteinopathy

Marta Gomez-Almeria [a,b,d], Loreto Martinez-Gonzalez [c,d], Ana Teresa Matos [f], Carmen Rodriguez-Cueto [a,b,d], Ana Rita Vaz [e,f], Raquel Martín-Baquero [a,b,d], Carmen Pérez de la Lastra [h], Rafael Infantes [e,f,g], Javier Fernández-Ruiz [a,b,d], Valle Palomo [d,h,i,j], Carmen Gil [c,d], Dora Brites [e,f], Ana Martinez [c,d], Eva de Lago [a,b,d,*]

[a] Instituto Universitario de Investigación en Neuroquímica, Departamento de Bioquímica y Biología Molecular, Facultad de Medicina, Universidad Complutense, Madrid, Spain
[b] Instituto Ramón y Cajal de Investigación Sanitaria (IRYCIS), Madrid, Spain
[c] Centro de Investigaciones Biológicas Margarita Salas-CSIC, Ramiro de Maeztu 9, 28040, Madrid, Spain
[d] Centro de Investigación Biomédica en Red de Enfermedades Neurodegenerativas (CIBERNED), Madrid, Spain
[e] Faculty of Pharmacy, Department of Pharmaceutical Sciences and Medicines, Universidade de Lisboa, 1649-003, Lisbon, Portugal
[f] Faculty of Pharmacy, Research Institute for Medicines (iMed.ULisboa), Universidade de Lisboa, 1649-003, Lisbon, Portugal
[g] Faculty of Medicine, Universidade de Lisboa, 1649-028, Lisbon, Portugal
[h] Instituto Madrileño de Estudios Avanzados en Nanociencia (IMDEA Nanociencia), C/Faraday 9, 28049, Madrid, Spain
[i] Unidad de Nanobiotecnología Asociada al Centro Nacional de Biotecnología (CNB-CSIC), Madrid, 28049, Spain
[j] Instituto de Investigación Sanitaria del Hospital Universitario La Paz (IdiPAZ), Paseo de la Castellana, 261, 28046, Madrid, Spain

ARTICLE INFO

Keywords:
Amyotrophic lateral sclerosis
Neuroinflammation
Neuroprotection
miRNAs
Protein kinase inhibitor
Riluzole
Combinatory therapy
TDP-43

ABSTRACT

Amyotrophic Lateral Sclerosis (ALS) is a devastating neurodegenerative disease for which no effective treatments currently exist. The FDA and EMA have approved only riluzole, a drug that modestly extends patient survival by 3–18 months. In our research, we have identified a novel CK1δ inhibitor, IGS2.7, which modulates TDP-43 proteinopathy, the main ALS pathological hallmark, in both patient-derived cellular models and TgTDP-43 mice. To assess the potential of IGS2.7 as a therapeutic candidate and considering riluzole remains the standard care for ALS patients, we evaluated its effects in combination with riluzole. Our results demonstrate that co-administration of IGS2.7 and riluzole at effective doses does not cause adverse effects. However, no additional therapeutic benefit was observed beyond that of IGS2.7 monotherapy, suggesting that IGS2.7 may be viable as either a stand-alone treatment or as an adjunct to riluzole. Notably, when suboptimal doses of both drugs were administered, a combined effect was observed. This suggests that, once IGS2.7 reaches clinical testing, its use together with lower doses of riluzole may enhance therapeutic efficacy while potentially minimizing side effects. Additional *in vivo* pre-clinical studies will be required to further evaluate this possibility, although only clinical trials will ultimately determine its clinical relevance.

1. Introduction

Amyotrophic Lateral Sclerosis (ALS) is a devastating neurodegenerative disorder of still unknown aetiology, which results in loss of upper and lower motor neurons (MNs), muscle paralysis, and death. Most cases of ALS are sporadic (90 %), while the rest are familial, with a genetic component (Feldman et al., 2022; Mitchell et al., 2013). Riluzole, approved in 1995 by the FDA, remains the most widespread therapeutic for the treatment of ALS patients (Bensimon et al., 1994; Saitoh and Takahashi, 2020), and the only approved in Europe

* Corresponding author. Instituto Universitario de Investigación en Neuroquímica, Departamento de Bioquímica y Biología Molecular, Facultad de Medicina, Universidad Complutense, Madrid, Spain.
E-mail address: elagofem@ucm.es (E. de Lago).

https://doi.org/10.1016/j.neuropharm.2025.110804
Received 4 October 2025; Received in revised form 26 November 2025; Accepted 8 December 2025
Available online 11 December 2025

(Ludolph et al., 2023). The treatment with riluzole at a dose of 100 mg, improves between 3 and 18 months overall survival and slightly slows the progression of symptoms (Fang et al., 2018). Edaravone that showed along with riluzole to slow disease progression in early-stage ALS patients (Seok, 2025) and the disease-modifying therapy Tofersen, for patients with SOD1 mutation, are also available for ALS, though their clinical benefits remain limited and still not approved by EMA.

Although there is great heterogeneity in clinical presentation, several shared mechanisms contribute to neurodegeneration and ALS disease progression in both sporadic and familial (genetic mutation) cases, such as, oxidative stress, neuroinflammation, mitochondrial dysfunction, altered synaptic function, excitotoxicity, and protein aggregation, among others (Feldman et al., 2022). Recent evidence in the ALS scientific community suggests this neurodegenerative disease as a TAR DNA-binding protein 43 (TDP-43)-pathy since more than 97 % of familial and sporadic ALS patients present TDP-43 aggregates in the cytoplasm of the affected cells (Babazadeh et al., 2023). Our research during the last decade is focused on the recovery of TDP-43 protein homeostasis with small molecules able to inhibit protein kinases involved in TDP-43 phosphorylation, the main post-translational modification found in TDP-43 aggregates (Palomo et al., 2021). Casein Kinase 1**δ** (CK1**δ**) was the first kinase described to phosphorylate TDP-43 *in vivo*; therefore, we developed brain-penetrant specific CK1**δ** inhibitors as a therapeutic strategy for treating ALS and other TDP-43 proteinopathies. The small molecule benzothiazole derivative known as IGS2.7 is a potent and selective protein kinase CK1**δ** inhibitor that exerts its neuroprotective effect by reducing TDP-43 hyperphosphorylation (Salado et al., 2014; Alquezar et al., 2016; Cuevas et al., 2024). MN survival and decreased reactive gliosis were observed in TDP-43 transgenic mice after IGS2.7 chronic administration (Martínez-González et al., 2020). Moreover, in sporadic ALS and FTD immortalised lymphocytes, IGS2.7 has been shown to recover TDP-43 homeostasis and functionality by decreasing TDP-43 phosphorylation and nuclear localization recovery (Salado et al., 2014; Alquezar et al., 2016). To translate this promising candidate into the clinic and considering that riluzole is the standard care for ALS patients, we here evaluated the therapeutic effect of IGS2.7 in combination with riluzole in our patient-based cellular model of lymphoblasts from sporadic ALS patients, whose previous characterisation revealed the presence of TDP-43 pathology (Posa et al., 2019), which showed to be safe and synergistic. The combined administration of the CK1**δ** kinase inhibitor IGS2.7 and riluzole at subeffective doses improved motor activity and preserved MNs in the spinal cord, while also counteracted the neuroimmune dysregulation in TDP-43 mice. Then, we propose IGS2.7, either as a single treatment or as an adjunct to standard riluzole therapy.

2. Materials and methods

2.1. Subjects and establishment of lymphoblastoid cell lines

Blood samples were collected with written informed consent from 5 sporadic ALS patients and 4 age-matched control subjects for CK1δ mRNA and protein determinations. All patients were diagnosed by applying the revised El Escorial criteria (Brooks et al., 2000) in the 12 de Octubre Hospital (Madrid, Spain). All procedures followed the National and European Union Guidelines and were approved by the Institutional Review Board of 12 de Octubre Hospital (CEIC02506), and the Ethics Committee of the Spanish National Research Council (CSIC) (protocol code 002/2020, May 19, 2021). Clinical information of control subjects and ALS patients is presented in Table 1. For the establishment of lymphoblastoid cell lines, Lymphoprep™ density-gradient centrifugation was applied to isolate peripheral blood mononuclear cells from blood samples according to the manufacturer's instructions (Axis-Shield Po CAS, Oslo, Norway). As previously described, lymphoblastoid cell lines were established by infecting peripheral blood lymphocytes with the Epstein–Barr virus (Ibarreta et al., 1997).

Table 1
Clinical information of control subjects and sporadic ALS patients.

Code	Gender	Age	Clinical presentation	Motor neuron affected
C100	Female	83	NA	NA
C105	Male	54	NA	NA
C106	Female	67	NA	NA
C108	Female	68	NA	NA
E2	Female	76	bulbar	SMN
E4	Female	53	bulbar	SMN + IMN
E6	Male	79	bulbar	IMN
E8	Male	55	respiratory	IMN
E10	Male	68	bulbar	NK

NA: not applicable; SMN, IMN: superior and inferior motor neuron (respectively); NK: Not known.

2.2. Cell culture and treatment of lymphoblast cell lines

Lymphoblasts were grown in suspension in RPMI medium (1×10^6 cells/mL) supplemented with 10 % (v/v) foetal bovine serum (FBS) and 1 % penicillin/streptomycin in T flask and maintained in a humidified 5 % CO_2 incubator at 37 °C. Cells were seeded at an initial concentration of 1×10^6 cells/mL. After 24 h, cells were treated with IGS2.7 (1 μM) and riluzole (1 μM) alone or in combination for a further 24 h period. Drugs were dissolved in DMSO and diluted in RPMI to ensure that the concentration of DMSO in the assay did not exceed 1 %.

2.3. Animals, experiments, and sampling

All experiments were conducted with male TDP-43(A315T) transgenic and male non-transgenic littermate sibling mice bred in our animal facilities from initial breeders B6, Cg-Tg(Prp-TARDBP*A315T) 95Balo/J) purchased from Jackson Laboratories (Bar Harbor, ME, USA). Mice were subjected to genotyping to identify the presence or absence of the transgene containing TDP-43(A315T) mutation (Wegorzewska et al., 2009). Animals were housed in a room with controlled lighting (08:00–20:00 lights on) and temperature (22 ± 1 °C) with free access to standard food and water. All animal experiments were approved by the ethical committees of our university and the regulatory institution (PROEX 201.8/22), being conducted according to European rules (Directive, 2010/63/EU) and following the ARRIVE guidelines. Then, once genotyped, wild-type (WT) and transgenic (Tg) mice were identified by numbered earmarks before the start of each experiment and randomly allocated to the different treatment groups. For data collection, all behavioural scoring was performed by researchers blinded to the animal genotype and treatment assignment. The same blinding was maintained for all histological analyses. In contrast, blinding was not considered to be necessary for the biochemical analyses due to the form in which the data were collected.

We performed two different sets of experiments, with effective or subeffective doses of the tested compounds. In the first experiment, we treated Tg mice with effective doses of riluzole (10 mg/kg/day) or IGS2.7 (1 mg/kg/day) alone or combined. Sub-effective doses (riluzole 5 mg/kg/day and IGS2.7 0.5 mg/kg/day) were selected based on an internal dose-response pilot study conducted in our laboratory to determine concentrations that did not produce measurable behavioural or histological effects in this model (data not shown). Effective doses were chosen based on our previously published work (Martínez-González et al., 2020; García-Toscano et al., 2025). In all cases, we treated WT and Tg male mice with vehicle (5.3 % Cremophor in saline solution) to serve as controls for the treatments and for the induction of the experimental pathology, respectively. In all cases, the compounds and the vehicle were administered intraperitoneally (i.p.), with treatment beginning at 65 days of age (presymptomatic stage) and continuing daily until the animals reached 95 days old (symptomatic stage), following the protocol used in our previous studies (Espejo-Porras et al., 2015; Rodríguez-Cueto et al., 2021). This also

included providing a special gel diet (DietGel®boost, ClearH20, Portland, ME, USA) during this period (see details in (Herdewyn et al., 2014a)). Actually, the TDP-43 (A315T) mice suffer from intestinal dysmotility, and the diet prevents sudden death and allows for phenotype progression (Herdewyn et al., 2014b). Throughout the treatment, animal weight gain was recorded along with performance in the rotarod test, a tool used to detect muscle weakness in these mice (Rodríguez-Cueto et al., 2021; Espejo-Porras et al., 2019). Following the two pharmacological experiments and immediately after the last behavioural recording, animals were euthanised by decapitation, and their spinal cords were dissected and removed. The lumbar spinal cord samples were rapidly frozen at −80 °C for reverse transcription quantitative real-time polymerase chain reaction (RT-qPCR). For histological analysis, samples were fixed in freshly prepared 4 % paraformaldehyde in 0.1 M PBS (pH 7.4) at 4 °C for one day, then cryoprotected in a 30 % sucrose solution for an additional day and finally stored at −80 °C before use for Nissl staining and immunohistochemical analysis.

2.4. Analysis of CK1δ activity and protein aggregation

CK1δ activity: Kinase-Glo® Luminescent Kinase Assay System (Promega, V6711) was used to perform CK1δ activity assays in the cell extracts. The assay used 50 ng of protein extracts from lymphoblasts or tissues from mice (frontal cortex and spinal cord), which were incubated with 1 mg/ml of casein (Sigma, Madrid, Spain) as substrate and 1 μM of ATP (Sigma, Madrid, Spain) in a final volume of 40 μL for 1 h at room temperature (RT). To stop the reaction, 40 μL of the kinase-glo reagent was added. Luminescence was measured after 10 min of incubation with the Promega™ GloMax® Plate Reader.

Protein aggregation: Aggregation assays were measured following a turbidometry methodology (Shmueli et al., 2017). Cells were seeded in a concentration of 1 million cells per mL and incubating with the different drugs at the desired concentration (5 μM IGS2.7, 5 μM riluzol, and 2 μM IGS2.7 + 2 μM riluzol) in DMSO for 24 h. DMSO concentration was always maintained below 1 % and used as vehicle. After treatment, the media was removed, and cells were washed with cold PBS. A cocktail of protease and phosphatase inhibitors was used for cell lysis and performing a centrifugation of 14000 g at 4 °C for 15 min.

Lysates were diluted to a concentration of 0.75 $g.L^{-1}$ using milliQ water and were incubated for a total time of 72 h at 37 °C, measuring turbidity every 24 h. Turbidity of the samples was quantified by absorbance measurements at 340 nm in cuvettes using a Cary 60 UV–Vis Spectrophotometer from Agilent Technologies. Each sample was gently shaken before recording and measured three times. Data was obtained for all absorbance measurements subtracting the value of the blank. Data was normalized to the median average of the controls for every experiment. In a typical assay, controls', patients' and treated patients' lymphoblasts were performed in the same experimental assay. At least three biological replicates (n = 3) were performed for all the data points obtained.

2.5. Behavioural recording

Rotarod test. Tg and WT mice were evaluated for motor weakness using the rotarod test with a LE8200 device (Panlab, Barcelona, Spain). Recordings were initiated just before starting the treatment (at 65 days of age) to have a reference value and repeated weekly during the whole treatment period. In each recording and after a period of acclimation and training (first session: 0 r.p.m. for 30 s; second and third sessions: 4 r.p.m. for 60 s, with resting periods of 10 min between sessions) conducted 30 min before, mice were tested with an acceleration from 4 to 40 r.p.m. over a period of 300 s and the time to fall off was quantified. Mice were tested for three consecutive trials with a rest period of approximately 15 min between trials, and the mean of the three trials was calculated.

2.6. Histological procedures and immunofluorescence analysis

Tissue slicing. Fixed spinal cords were sliced with a cryostat at the lumbar level (L4-L6) to obtain coronal sections (20 μm thick) that were collected on gelatine-coated slides.

The collected spinal cord sections were processed for Nissl staining and immunofluorescence.

Nissl staining. Slices were stained with cresyl violet following a previously described protocol (Alvarez et al., 2008), enabling the identification and quantification of spinal MN cell bodies. A Leica DMRB microscope was used for tissue examination, and images were captured with a DFC300Fx camera (Leica, Wetzlar, Germany).

To quantify Nissl-stained MNs (>400 μm^2) in the ventral horn, high-resolution photomicrographs were taken using a 10 × objective under consistent lighting, brightness, and contrast conditions. Neuron counting was performed using ImageJ software (U.S. National Institutes of Health, Bethesda, Maryland, USA, http://imagej.nih.gov/ij/, 1997–2012). At least three sections per animal were analysed, with four images per section. The analysis was conducted by researchers blinded to the treatment groups to determine the mean neuron count for each group.

2.6.1. Immunofluorescence

For *lymphoblast cell line* analysis, cells were adhered to coverslips coated with a solution of 0.25 % Gelatin (Sigma, Madrid, Spain) for 30 min at RT followed by a solution of 1 mg/mL poly-L-lysine (Sigma, Madrid, Spain) diluted 1:50 in Borax buffer ($Na_2B_4O_7{\cdot}10H_2O$ 15 mM, pH 8.4) overnight at 37 °C. Once the cells were attached, they were fixed with 4 % paraformaldehyde for 30 min, permeabilised with 0.5 % Triton X-100 in PBS for 10 min, and blocked with 0.5 % BSA for 1 h at 37 °C.

Table 2
Antibodies used in this work.

Primary Antibody	Species	Dilution (WB/IF)	Supplier (Catalog#)
TDP-43	Rabbit	1:1000/NA	Proteintech (10782-2-AP)
TDP-43	Mouse	1:1000/1:100	Proteintech (67345-1-Ig)
p(Ser409/410)-TDP-43	Rabbit	1:500/NA	Proteintech (22309-1-AP)
CK1δ	Mouse	1:1000/NA	Santa Cruz Biotech (sc-55553)
GAPDH	Rabbit	1:1000/NA	Cell Signal (5174)
GFAP	Rabbit	NA/1:200	Dako Cytomation (Z0334)
STMN2	Rabbit	1:1000	Novusbio (NBP1-49461)
Iba-1	Rabbit	NA/1:500	Wako Chemicals (019–19741)

Secondary Antibody	Immunological Procedure	Dilution	Supplier (Catalog#)
Goat anti-mouse IgG HRP conjugate	WB	1:7000	Bio-Rad (1706516)
Goat anti-rabbit IgG HRP conjugate	WB	1:7000	Bio-Rad (1706516)
anti-mouse Alexa 488	IF	1:1000	Molecular Probes (A-11001)
anti-rabbit Alexa 488	IF	1:200	Molecular Probes (A21206)

NA: not applicable, WB: Western blotting, IF: Immunofluorescence; HRP: Horseradish Peroxidase.

Samples were incubated with primary antibodies (Table 2) for 60 min at 37 °C. After removing the primary antibody, cells were washed with PBS and incubated with Alexa Fluor 488-conjugated antibody (Table 2). DAPI (1:1000, Sigma) was used for nuclear staining. Preparations were mounted with Fluor Save reagent (Calbiochem, Madrid, Spain), and high-resolution images were acquired with the LEICA TCS SP5 confocal microscope (100x oil immersion objective). Leica Application Suite X (version 3.5.7.23225) and Image J software (version 1.53K) were used to analyse images.

For *spinal cord*, slices were used for the detection and quantification of astrocytic glial fibrillary acidic protein (GFAP) and the microglial ionized calcium-binding adaptor molecule 1 (Iba-1). After preincubation for 1 h with Tris-buffered saline with 1 % Triton X-100 (pH 7.5), sections were sequentially incubated overnight at 4 °C with: (i) a polyclonal anti-GFAP (1:200; Dako Cytomation, Glostrup, Denmark); (iii) a polyclonal anti-Iba-1 (1:500; Wako Chemicals, Richmond, VI, USA) antibody, followed by washing in Tris-buffered saline and incubation (at 37 °C for 2 h) with an anti-rabbit secondary antibody made in donkey (1:200; Biolegend, San Diego, CA, USA), conjugated with Alexa 488 (Invitrogen, Carlsbad, CA, USA) rendering green fluorescence for both anti-GFAP and anti-Iba-1. Imager M2 microscope (Zeiss, Oberkochen, Germany) was used for slide observation and photography. For quantification, high-resolution digital microphotographs were taken with the 10 × objective under the same conditions of light and brightness and contrast. They were used to measure the mean density of labelling in a selected area using the ImageJ software. All data were expressed in arbitrary units.

2.7. RT-qPCR analysis

In the case of *lymphoblast samples*, RNA extraction, cDNA synthesis, and quantitative polymerase chain reaction (PCR) were carried out as previously described (Cuevas et al., 2022). RT-qPCR was performed using the Light Cycler® 96 System (Roche, Mannheim, Germany) and the associated software following the manufacturer's instructions. Each reaction was conducted with 20 ng of cDNA using FastStart Essential DNA Green Master (Roche, Mannheim, Germany). Biological triplicates were performed. The primers sequences used were: Forward Human 1 CSNK1D (TTGTATCGCCACTGTATTTG) and Reverse Human 1 CSNK1D (TGGGAAGAAAGGTAGAAGTC), both from Sigma-Aldrich. Data analysis was based on the ΔΔCT method, normalizing the raw data to the hRPS17 housekeeping gene.

In the case of *mouse sample experiments,* for the determination of inflammatory-associated miRNAs (spinal cord), as well as genes and axonal transport/synaptic degenerative markers (spinal cord), samples were homogenized in Trizol reagent (Invitrogen, Waltham, MA, USA) using a Pellet Mixer (VWR Life Science, EUA). The total RNA was extracted and quantified on a NanoDrop ND100 Spectrophotometer (NanoDrop Technologies, Wilmington, DE, USA) according to the standard procedure in our laboratory (Barbosa et al., 2021).

For the determination of miRNA expression, 5 ng/μL of total RNA was converted into cDNA using miRCURY LNA™ Universal RT kit (QIAGEN, Valencia, CA, USA) under controlled conditions: 60 min at 42 °C followed by heat-inactivation of the reverse transcriptase for 5 min at 95 °C and subsequent cooling to 4 °C for 24 h. RT-qPCR was performed on a QuantStudio 7 Flex Real-Time PCR System, using PowerSYBR® Green PCR Master Mix (Applied Biosystems, Life Technologies, Waltham, MA, USA) with pre-designed primers (listed in Table S1). PCR was performed in 384-well plates, with each sample performed in duplicate, and a non-template control (NTC) was included for each amplification product. SNORD110 (reference gene) was used as an endogenous control. The miRNA RT-qPCR running conditions were 10 min at 95 °C for polymerase activation/denaturation, 50 amplification cycles at 95 °C for 10 s, and 60 °C for 1 min (ramp-rate of 1.6°/s).

For gene expression, 1000 ng/μL of total RNA was converted into cDNA using the Xpert cDNA Synthesis Supermix Kit under controlled conditions: 5 min at 65 °C followed by 10 min at 25 °C to incubate the samples, 15 min at 50 °C, 5 min at 85 °C to inactivate the enzyme and final cooling to 4 °C for 24 h. RT-qPCR was performed on a QuantStudio 7 Flex Real-Time PCR System, using Xpert Fast SYBR Mastermix (Uni) BLUE with pre-designed primers (listed in Table S2). The PCR was performed in 384-well plates with each sample measured in duplicate, and NTC was included for each amplification product. β-actin was used as an endogenous control to normalize gene expression levels. RT-qPCR running conditions were 50 °C for 2 min and 95 °C for 2 min, followed by 50 amplification cycles at 94 °C for 5 s and 62 °C for 30 s. The expression of mRNA/miRNA was measured via the $2^{-\Delta\Delta Ct}$ method relative to that of WT treated with vehicle. Target genes for miRNAs found significantly altered in the transgenic mice upon treatments will be predicted using miRNet database (https://www.mirnet.ca/). Gene Ontology (GO) functional analysis enrichment will be carried out and classified into biological process (BP), molecular function (MF), and cellular component (CC) in the miRNet platform. p value < 0.05 and gene counts (hits) ≥ 6 will be considered as significant.

2.8. Western blot analysis

For *lymphoblast cell lines*: Cells were harvested, washed in PBS, and then lysed in ice-cold lysis buffer solution [50 mM Tris-HCl pH 7.4, 15 mM $MgCl_2$, 150 mM NaCl, 5 mM EDTA, 0.5 % (v/v) sodium deoxycholate, 0.5 % (v/v) NP-40 and 0.1 % (v/v) SDS)], containing 1 mM sodium orthovanadate, 1 mM phenylmethylsulfonyl fluoride (PMSF), 1 mM sodium pyrophosphate and protease inhibitor mixture. The protein content was quantified with the Pierce BCA Protein Assay kit (Thermo Scientific). Equal amounts of proteins (30–50 μg) were fractionated on a SDS polyacrylamide gel by electrophoresis and then transferred to PVDF membranes with the Trans-Blot Turbo Transfer System (Bio-Rad). Membranes were then blocked for 1 h with 5 % bovine serum albumin (BSA) in PBS and incubated with primary antibodies (Table 2) overnight at 4 °C. After 1 h incubation time with species-specific antibodies conjugated with horseradish peroxidase (Bio-Rad), chemiluminescent was measured by using a chemiluminescent substrate detection system ECL and the Chemidoc Imaging System (Bio-Rad, Alcobendas, Madrid, Spain). Image J software (National Institutes of Health, Bethesda, MD, USA) was used to quantify relative bands intensities.

For spinal cords: spinal cords were lysed in RIPA buffer supplemented with a protease and phosphatase inhibitor cocktail (Roche, Mannheim, Germany). The protein content of the extracts was determined by the Pierce BCA Protein Assay kit (ThermoFisher, Madrid, Spain). Equal amounts of proteins were resolved by SDS-polyacrylamide gel electrophoresis (TGX Stain-free™ Gel Fast Cast; BioRad Laboratories, Hercules, CA), transferred to polyvinylidene fluoride (PVDF) membranes (Immobilon-P, Millipore, Bedford, MA) and immunodetected, as previously described (Espejo-Porras et al., 2015). The primary antibodies and dilutions are listed in Table 2. Signals from the primary antibodies were amplified using species-specific antisera antibodies conjugated with horseradish peroxidase and detected with a chemiluminescent substrate detection system ECL (Bio-Rad, Alcobendas, Madrid, Spain). Relative band intensities were quantified using a ChemiDoc station with Quantity One 1D analysis software (Bio-Rad Laboratories, Madrid, Spain). Data were calculated as the ratio between the optical densities of the specific protein band and the total protein measured in membranes and then normalized as percentages over the WT animals treated with vehicle (Espejo-Porras et al., 2015).

2.9. Statistical analysis

Sample size was determined using a power calculation (GRANMO calculator), which indicated that a minimum of 8 animals per group was required to achieve 80 % power at $\alpha = 0.05$. Graph Pad Prism software version 10 (La Jolla, CA, USA) was used for statistical analysis. Statistical significance was estimated using a two-tailed Student's *t*-test for comparisons between two groups or one-way ANOVA followed by the

indicated post-hoc analysis for multiple comparisons in each case. Whenever outliers were found, they were removed from the datasets to ensure the accuracy and robustness of the statistical analyses. A p-value <0.05 was considered statistically significant.

3. Results

3.1. Immortalised lymphocytes from sALS patients present upregulated expression and activity of CK1δ

In previous work, we demonstrated the usefulness of lymphoblastoid cell lines in studying central nervous system (CNS) diseases, as they reflect the pathological fingerprints found in the CNS during disease progression (Posa et al., 2019; Cuevas et al., 2022; Vaca et al., 2021). Lymphoblasts from sporadic ALS (sALS) patients, whose previous characterisation revealed the presence of TDP-43 pathology (cytoplasmic accumulation, fragmentation, and hyperphosphorylation of TDP-43), represent a suitable platform to screen promising ALS therapies (Pansarasa et al., 2018).

To provide a personalised characterisation of the disease and based on our previous work, where we found an upregulation of CK1δ expression in the spinal cord and frontal cortex of post-mortem samples from sALS patients (Martínez-González et al., 2020), we decided to analyse CK1δ mRNA and protein expression levels in 5 lymphoblastoid cell lines (LCLs) derived from sALS patients and 4 LCLs derived from healthy donors, as controls. After 24 h of lymphoblast synchronisation, we extracted both mRNA and the protein content. RT-qPCR analysis showed a significant increase in CK1δ mRNA expression in sALS lymphoblasts compared to controls (Fig. 1A). Related to protein expression, WB analysis revealed higher CK1δ protein levels in sALS samples than in those from healthy donors (Fig. 1B).

Furthermore, we assessed CK1δ activity with the Kinase-Glo assay kit. Protein extracts from lymphoblasts were incubated with casein (CK1δ substrate) and adenosine triphosphate (ATP) for 1 h. The kinase activity was determined by the luminescence detected at the end of the experiment, which is correlated with the remaining ATP. In all ways, increased CK1δ activity in sALS lymphoblasts was noticed compared to controls ($p < 0.05$) (Fig. 1C). Therefore, the enhanced CK1δ mRNA and protein expression, together with the higher activity observed in sALS lymphoblasts compared to healthy subjects, reinforces the notion that this human cellular model is suitable to screen the therapeutic efficacy of CK1**δ** inhibitors.

3.2. IGS2.7 alone or in combination with riluzole is effective in supporting TDP-43 homeostasis and reducing protein aggregation in sALS lymphocytes

Prior research has demonstrated the effectiveness of the CK1δ kinase inhibitor IGS2.7 in recovering TDP-43 protein homeostasis and functionality in human cell-based and animal TDP-43-pathy models (Salado et al., 2014; Alquezar et al., 2016; Martínez-González et al., 2020). These beneficial effects are derived from its ability to reduce TDP-43 aberrant phosphorylation and to restore its nuclear localization.

To strengthen the translational value of this CK1**δ** inhibitor towards the clinical scenario, we decided to investigate whether the beneficial effects shown by IGS2.7 in immortalised lymphocytes from sALS patients are potentiated when it is combined with riluzole, the most used drug to treat ALS patients today. To assess the synergistic effect, we evaluated the efficacy of the drugs both individually and in combination at submaximal doses. Results showed a decrease in the aberrant phosphorylation of TDP-43 when cells were treated with IGS2.7 alone and in combination with riluzole compared with cells treated with vehicle. This effect was more pronounced when both drugs were administered simultaneously (Fig. 2A). No significant effect was found with riluzole alone at 1 μM, probably due to the high variability encountered among patient samples. We then analysed the subcellular localization of the TDP-43 protein, revealing that the cytoplasmic localization of TDP-43 is notable in the ALS lymphoblasts as compared with the control ones. All the tested treatments restore the nuclear localization of TDP-43, compared with the untreated ALS lymphoblasts. However, this recovery was more effective upon treatment either with the compound IGS2.7 or the cotreatment relative to cells that just received riluzole (Fig. 2B). To assess the functional homeostasis of TDP-43, we examined the expression of stathmin-2 (STMN2), whose mRNA splicing is regulated by TDP-43 (Krus et al., 2022). STMN2 is known to be reduced in the spinal cord of most patients with ALS. As shown in Fig. 2C, STMN2 levels are

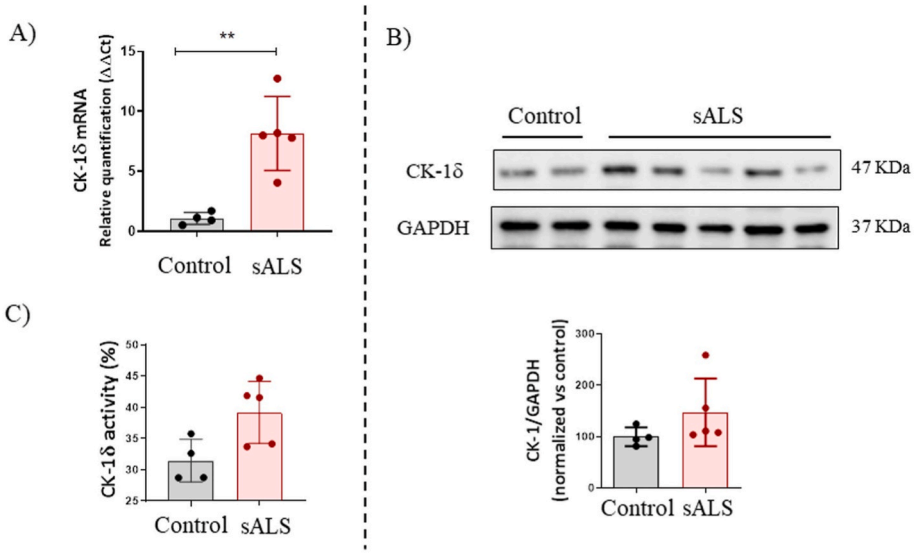

Fig. 1. CK1δ mRNA, protein expression levels and activity in immortalised lymphocytes from four control subjects and five sporadic ALS (sALS) patients. A) CK1δ mRNA expression was analysed by quantitative RT-PCR. RPS17 was used as the housekeeping gene. Dots represent the mean ± standard deviation (SD) of two independent triplicated experiments. B) Representative immunoblots and densitometric quantification of CK1δ protein expression. GAPDH was used as the loading control. Dots indicate the mean ± SD of two independent experiments. C) CK1δ activity performed with Kinase-Glo system in lymphoblast cell extracts. Dots indicate the mean (%) ± SD of three independent experiments conducted in triplicate. Statistical analyses were performed using one-way ANOVA and *post hoc* Bonferroni's test (**$p < 0.01$). CK1δ, casein kinase 1 delta; GAPDH, Glyceraldehyde-3-phosphate dehydrogenase.

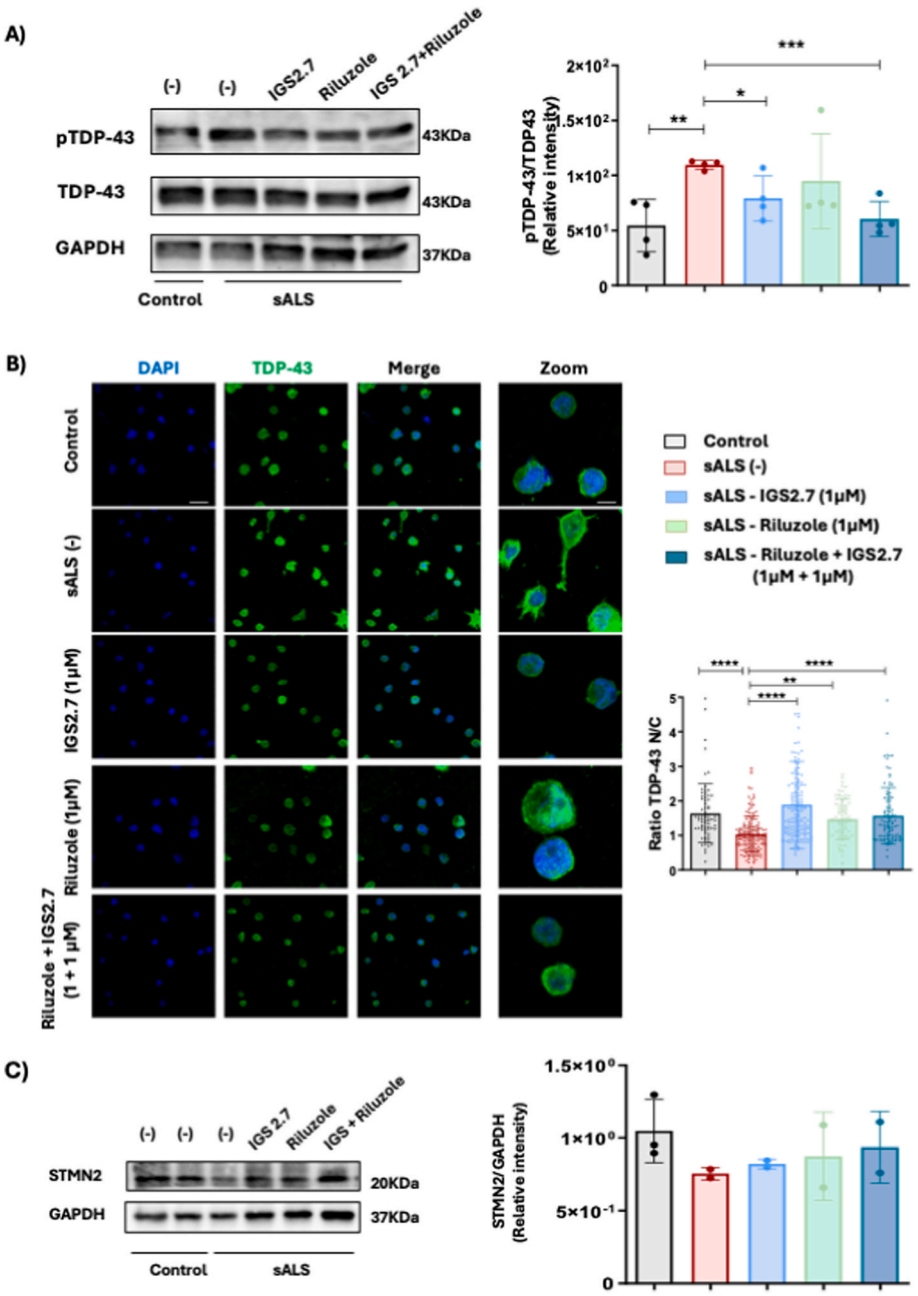

Fig. 2. TDP-43 phosphorylation and localization status in ALS and control lymphoblasts after treatment with IGS2.7 and riluzole alone and in combination. Cells were incubated for 24 h in the presence of IGS2.7 (1 μM), riluzole (1 μM), or IGS2.7 + riluzole (1 μM + 1 μM). A) Representative immunoblots are shown. Densitometric quantification of pTDP-43 was normalized against total TDP-43. B) Representative confocal immunofluorescence images show TDP-43 subcellular localization. Cells were stained with anti-TDP-43 antibody (green) and DAPI (blue). Scale bar, 20 μm. Magnified cells from images are shown for better visualization. Fluorescence intensity was evaluated in at least four fields of view in two independent experiments, each including four controls and four ALS patients. Graph represents single-cell TDP-43 nucleus-cytoplasm ratio. C) Protein levels of STMN2. Data were assessed by one-way ANOVA and *post hoc* Bonferroni's test (*$p <$ 0.05, **$p < 0.01$, ***$p < 0.001$, ****$p < 0.0001$). pTDP-43, phospho-TAR DNA-binding protein 43; TDP-43, TAR DNA-binding protein 43; STMN2, stathmin 2). (For interpretation of the references to colour in this figure legend, the reader is referred to the Web version of this article.)

significantly decreased in sALS-derived LCLs compared with control cells. Importantly, STMN2 expression increases after treatment, with the greatest recovery observed following the combined administration of IGS2.7 and riluzole. These results indicate that restoring TDP-43 nuclear localization contributes to the normalization of STMN2 levels, supporting the recovery of TDP-43–dependent cellular functions.

The combined treatment was found to be synergistic and more effective in decreasing TDP-43 hyperphosphorylation, though IGS2.7 alone was more effective in supporting TDP-43 nuclear localization. Therefore, IGS2.7 is a promising therapy for treating ALS not only as a single treatment but also as an add-on to riluzole standard care.

We also wanted to investigate, one of the main pathological hallmarks of ALS: the accumulation of misfolded or aggregated proteins forming inclusions in the cytoplasm of the affected cells. These aggregates can include phosphorylated, ubiquitinated, and cleaved forms of TDP-43 protein. To evaluate the protein aggregation levels in ALS lymphoblasts, we have established a turbidity assay (Pérez de la Lastra Aranda et al., 2024) that measures total proteome content in cell extracts. For these experiments, we have used 3 subjects as controls and 5 lymphoblast cell lines derived from sALS patients. Protein extracts from

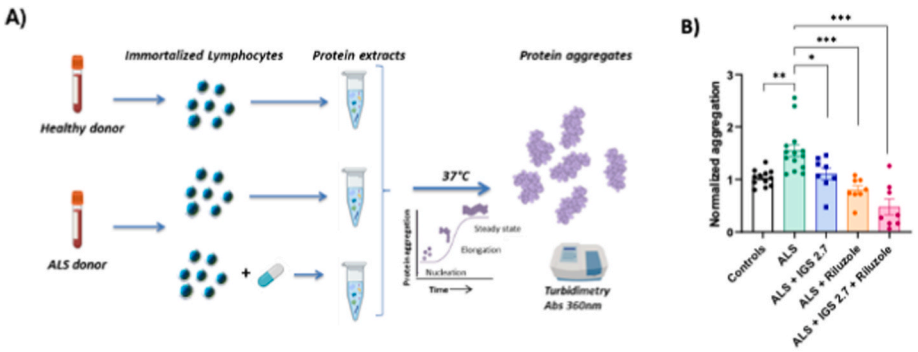

Fig. 3. Total proteome aggregation in ALS and control lymphoblasts after treatment with IGS2.7 and riluzole alone and in combination. A) Representation of methodology. B) Normalized absorbance measurements of sporadic ALS patient (sALS) lymphoblasts with or without pharmacological treatment at 72 h. Each of the points depicted in the graph represents 3 biological replicates of the experiment. Statistical analysis was performed through One-way ANOVA with Dunnett comparison test, comparing the mean of each column to the mean of sALS (#: $p < 0.1$, *: $p < 0.05$, **: $p < 0.01$; ***: $p < 0.001$).

immortalised lymphocytes were incubated at 37 °C for 72 h; then absorbance was measured to determine proteome turbidity (Fig. 3A). We noticed an elevated protein aggregation in all the lymphoblast samples from sALS patients in terms of global proteome turbidity, as compared to healthy donors (Fig. 3B). We next performed the assay after treating the lymphoblasts with IGS2.7, riluzole, or a combination of both drugs for 24 h. We observed a significant decrease in the protein aggregation turbidity when cells were exposed to IGS2.7, or riluzole, but a synergistic effect and increased reduction when both drugs were administered at the same time (Fig. 3B). Therefore, the compounds presented a synergistic effect in lowering total protein aggregation.

3.3. Administration of IGS2.7 alone or in combination with riluzole exerts a synergistic neuroprotective effect in the TDP-43 (A315T) transgenic mouse model

To assess the treatment effects of the kinase inhibitor IGS2.7 and riluzole, alone or combined, we performed two sets of experiments in the Pr-TDP43(A315T) Tg mouse model. Firstly, we examined if the activity of CK1δ was dysregulated in the CNS of these mice. We analysed two different CNS regions, the spinal cord and the cerebral cortex. Results obtained using the kinase Glo methodology showed a significant increase in kinase activity in both CNS tissues (Fig. 4A), reinforcing the potential of the Tg mice for CK1δ inhibitors evaluation.

Doses for the first experiment in the Pr-TDP43(A315T) mouse model were selected based on our previous results (Fig. 4B). Thus, the dose initially chosen for IGS2.7 was 1 mg/kg i.p., which showed neuroprotective and anti-inflammatory properties in the TPD43(A315T) Tg mice (Martínez-González et al., 2020). Furthermore, we selected a riluzole dose of 10 mg/kg i.p., based on previous reports in other ALS mouse models, such as the classical SOD1(G93A) model (Jaiswal, 2017) and a dose-response pharmacological study conducted in our laboratory in the TDP43(A315T) model (García-Toscano et al., 2025).

Co-administration of IGS2.7 and riluzole at effective doses produced a neuroprotective effect (Fig. 4C) on dorsal horn MNs, like that observed with separate administration of each compound compared to vehicle-treated Tg mice. Likewise, no additive effect on gliosis reduction was observed when using the combination compared to the single administration of each compound (Fig. 4C). No behavioural changes were detected in the rotarod test for any of the Tg mouse groups (data not shown). Notably, no synergistic or adverse effects were observed with the co-administration of IGS2.7 and riluzole at the studied doses and

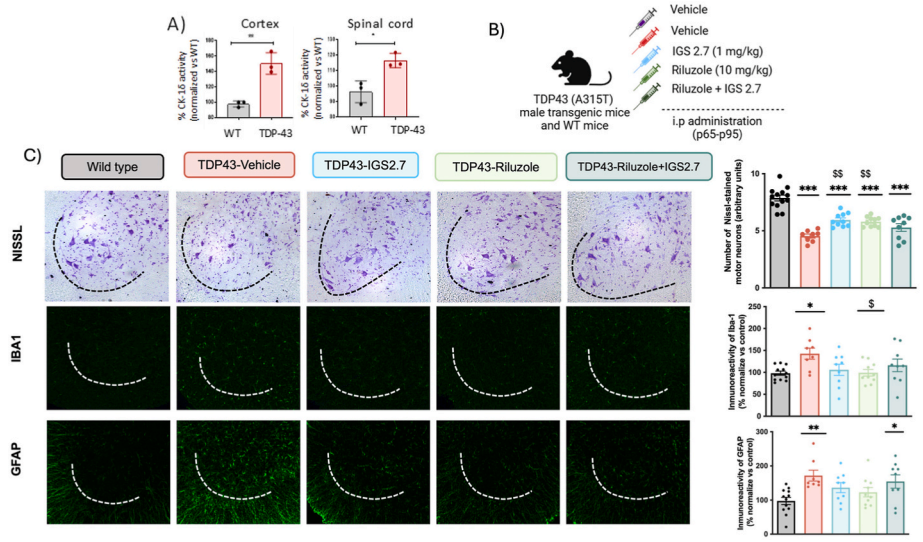

Fig. 4. CK1δ activity in CNS tissues from TDP43(A315T) Tg mice and the anti-inflammatory and neuroprotective effects of treatment with IGS2.7, riluzole or their combination in the spinal cord. A) CK-1δ activity performed with Kinase-Glo system in spinal cord and cerebral cortex samples from TDP43(A315T) Tg (Tg) or wild-type mice (WT). B) Scheme of the experimental design including times and doses of each treatment. C) Quantification of Nissl staining, and Iba1 and GFAP immunoreactivity, including representative images (scale bar = 100 μm), in the lumbar ventral horn of the spinal cord in TDP43(A315T) Tg and WT mice. Values are means of 8–11 animals per group. Data were assessed by two-way analysis of variance (*$p < 0.05$, **$p < 0.01$, ***$p < 0.005$ vs WT-vehicle mice; $^{\$}p < 0.05$, $^{\$\$}p < 0.01$ vs. Tg TDP43(A315T) mice). GFAP, glial fibrillary acidic protein, Iba1, Ionized calcium-binding adaptor molecule 1.

conditions.

In a second experiment, we conducted a new *in vivo* study to better assess the potential synergistic effects of combining IGS2.7 and riluzole, using sub-effective doses of each compound. Specifically, we administered IGS2.7 at 0.5 mg/kg and riluzole at 5 mg/kg, either alone or in combination, to male Tg mice, from p65 to p95 (Fig. 5A). As expected, no effects on weight evolution were observed throughout the treatment period (Fig. 5B). Likewise, a non-significant trend toward improvement in the rotarod test was noted after three weeks of treatment in the Tg mouse group treated IGS2.7-riluzole combination (Fig. 5C). The overall reduction in motor function observed in TDP-43 Tg mice in the rotarod test ($p < 0.05$), relative to the WT mice, was not significantly improved by any of the sub-effective treatments (Fig. 5C). Interestingly, performance in the rotarod test appears to worsen following four weeks of riluzole treatment alone ($p < 0.01$, Fig. 5C). Once again, a slight but non-significant amelioration was observed after one month of combined treatment.

After treatment, on postnatal day 95, animals were sacrificed. Histological analysis of spinal cord samples from TDP-43(A315T) Tg mice revealed MN loss, which was not prevented by the administration of IGS2.7 or riluzole at sub-effective doses (Fig. 6). However, the combination of both drugs significantly preserved MN viability compared to untreated Tg mice ($p < 0.001$), although it did not reach the levels observed in the WT mice ($p < 0.001$). These results indicate a synergistic effect of the combined treatment. No differences in the microglial Iba-1 immunoreactivity were detected between the WT and the Tg mice, regardless of treatment with riluzole or IGS2.7 (Fig. 6). Interestingly, the combined treatment led to an increase in microglia Iba-1 staining compared to WT mice ($p < 0.01$) and Tg mice treated with IGS2.7 alone ($p < 0.05$). Additionally, while the astrocytic GFAP marker showed higher levels in the vehicle-treated TDP43(A315T) Tg mice, these elevated levels persisted across all treatment conditions, with no significant differences observed (Fig. 6).

3.4. Administration of IGS2.7, riluzole, or their combination counteract the compromised neuron-glia homeostasis in the TDP-43(A315T) transgenic mouse model

With the main goal to explain microgliosis and astrocytosis observed in the previous experiments, we next evaluated common inflammation-associated genes (Fig. 7A). First, we assessed astrocyte reactive markers, such as *Gfap* and *S100b*, and noticed that both were upregulated in this mouse model ($p < 0.01$, Fig. 7B). All the treatments that were tested led to a marked decrease of gene expression levels to values like control ones, suggesting protection over astrocyte activation.

We further noticed that genes that code for axonal transport proteins (e.g., dynein and kinesin) and for synaptic proteins (synaptophysin and PSD-95) were downregulated in the TDP-43 mouse model (at least $p < 0.05$, Fig. 7C). Interestingly, all the treatments showed efficacy in upregulating the gene expression toward control levels (at least $p < 0.05$), thus counteracting neurodegeneration.

Microglial subtypes have been extensively researched in the context of ageing and disease. Genes such as Cx3Cr1, P2ry12, and Tmem119 were shown to be highly expressed in homeostatic microglia (Taketomi and Tsuruta, 2023). We found an increase of *Cx3cr1* in the Tg mice, together with a decrease of *P2ry12* and *Tmem119* (at least $p < 0.05$, Fig. 7D). IGS2.7, riluzole and their combination with IGS2.7 reversed *Cx3cr1* gene expression upregulation in the mouse model to levels of the WT mice (at least $p < 0.05$). Downregulation of *P2ry12* and *Tmem119* in the TDP-43 mice ($p < 0.0001$) was counteracted by riluzole and IGS2.7 + riluzole (at least $p < 0.05$).

Finally, a set of inflammation-associated markers, such as *Arginase*, *Hmgb1*, and *iNOS*, were found overexpressed in the mouse model (at least $p < 0.05$, Fig. 7E). To note that no significant alterations were induced in the TARDP mRNA levels with any of the treatments (Fig. 7F).

IGS2.7 and its combination with riluzole revealed success in sustaining Arginase normal values. Similar enhanced results were obtained for *Hmgb1* and *iNOS* in the TDP-43 model, and this time, all treatments were effective in preventing changes from occurring with values similar to control ones.

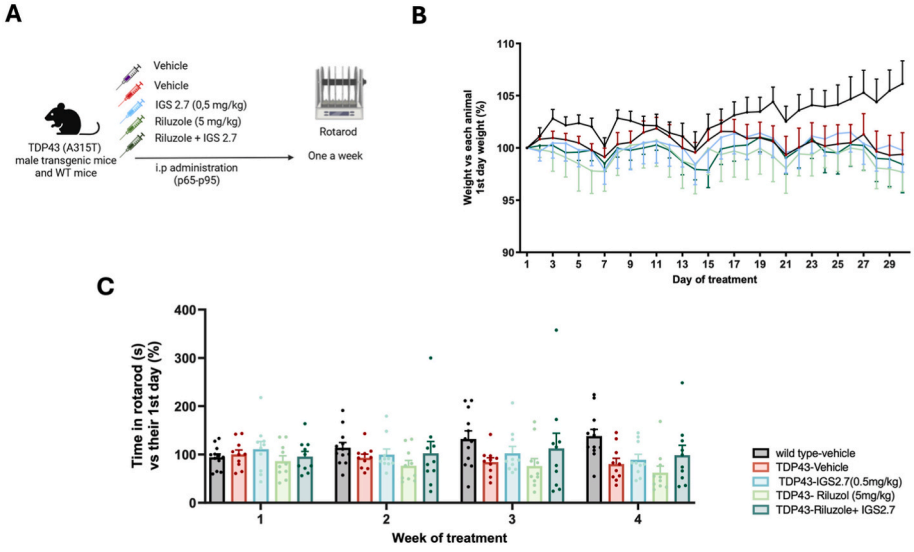

Fig. 5. Phenotypic characteristics of TDP43(A315T) Tg mice treated with IGS2.7, riluzole or combination of both drugs A) Scheme of experimental design including times and doses of each treatment (subeffective doses of IGS2.7, riluzole, or combination). B) Animal weight and C) rotarod performance of TDP43(A315T) Tg and WT male mice after the daily treatment with IGS2.7 (0.5 mg/kg), riluzole (5 mg/kg), combination, or vehicle from p65 to p95. In all cases, values are means ± SEM of 8–11 animals per group. Data were assessed by repeated measures of two-way ANOVA (*$p < 0.05$ vs. WT).

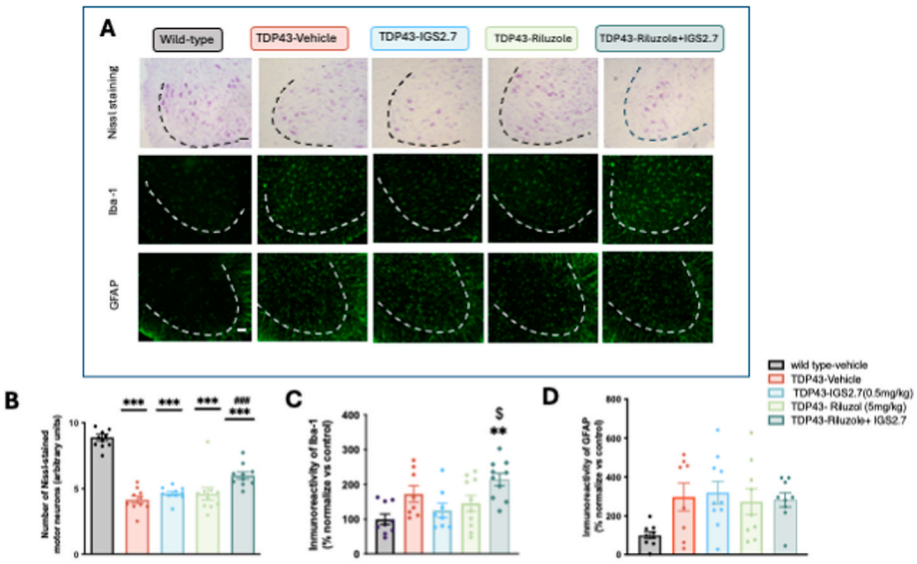

Fig. 6. Anti-inflammatory and neuroprotective effects of treatment with subeffective doses of IGS2.7, riluzole, or their combination in the spinal cord. A) Representative images and B) quantification of Nissl staining, C) Iba1 and D) GFAP immunoreactivity (scale bar = 100 μm), in the lumbar ventral horn of the spinal cord in TDP43(A315T) Tg and WT mice. Values are mean of 8–11 animals per group. Data were assessed by two-way analysis of variance (**p < 0.01, ***p < 0.005 vs. WT-vehicle mice; $^{\$}$p < 0.05 vs. TDP43 Tg mice). GFAP, glial fibrillary acidic protein, Iba1, Ionized calcium-binding adaptor molecule 1.

3.5. The combination of IGS2.7 with riluzole modulates dysregulated miRNAs in the TDP-43(A315T) transgenic mouse model

Previous studies have shown that miR-124, miR-146a, miR-21, miR-155 and miR-125b are upregulated in the spinal cord of symptomatic SOD1(G93A) mice, correlating with neurodegeneration and inflammatory status (Cunha et al., 2018). Additionally, other miRNAs, such as miR-129-5p, miR-221-3p, miR-3065-5p, miR-204-5p and miR-183-5p, have been identified as key factors in cytoplasmic TDP-43 inclusions and ALS pathology (Pegoraro et al., 2017; Loffreda et al., 2020; Paez-Colasante et al., 2020a; Li et al., 2020). Based on these findings, we hypothesised that some of these miRNAs might also be dysregulated in our TDP-43 mouse model and responsive to therapeutic intervention.

To test this, we analysed the spinal cord of the symptomatic TDP43 (A315T) Tg mice treated with subeffective doses of IGS2.7, riluzole or their combination (Fig. 5A). Our results revealed a significant upregulation of miR-124, miR-146a, miR-221, and miR-3065 in TDP-43 mice compared to vehicle-treated WT mice ($p < 0.05$, Fig. 8), while no significant alterations were observed for the other miRNAs (Supplementary Fig. S1).

Next, we evaluated the impact of our treatments on these dysregulated miRNAs. All treatment conditions exerted a normalizing effect on miR-124 levels, with the combination of IGS2.7 and riluzole showing the strongest effect ($p < 0.001$), by restoring levels close to those of control mice. However, miR-146a levels remained upregulated under any treatment, though the combination therapy showed a trend toward reduction. Regarding miR-221, only the combination of IGS2.7 and riluzole successfully restored its control levels. Finally, both riluzole and its combination with IGS2.7 significantly normalized miR-3065 levels ($p < 0.05$).

Regarding miR-221, only the combination of IGS2.7 and riluzole successfully restored its control levels, while both riluzole and its combination with IGS2.7 significantly normalized miR-3065 levels ($p < 0.05$).

To further understand the significance of our data, we decided to predict the potential target genes of the miRNAs that were found significantly modified in the TDP-43 mice and regulated upon treatment with riluzole plus IGS2.7, i.e., miR-124-3p, miR-221-3p, and miR-3065-5p. For that, we used the miRNet database (https://www.mirnet.ca/). The miRNet online tool predicted 1969 target genes for the three selected miRNAs. To explore the biological pathways possibly affected by the target genes, a functional enrichment analysis of the target genes was carried out by using pathway maps from the Gene Ontology (GO) repository. GO terms were investigated for biological processes, cellular components, and molecular function processes associated with the set of predicted and validated target genes found for those 3 selected miRNAs, which are depicted in Fig. 8B. In the biological process category, among the top and significant GO terms, all the three miRNAs were related to inflammatory processes, neuronal and glial related functions, and protein kinase activity, as represented in Supplementary Fig. S2 miR-124-3p is by far the major gene target regulatory one, followed by miR-221-3p and at last the miR-3065-5p. Therefore, the modulation of these triad of miRNAs may account to the regulation of genes involved in protein kinase activity, in inflammation, gliogenesis, and neuron-related processes.

4. Discussion

Currently, riluzole is the only treatment for ALS authorised in the EU, offering limited effects on disease progression. Patients also receive supportive care to alleviate symptoms, including physical, occupational, and speech therapy, as well as respiratory support. For patients with the genetic SOD1-ALS subtype, Tofersen (Qualsy®), an antisense oligonucleotide targeting SOD1 mRNA, has recently received conditional marketing authorisation in the EU, while retaining orphan drug status. Due to the clinical and pathological heterogeneity of ALS, there is a pressing need for therapies that preserve muscle function and prolong survival. This may be achieved through multitarget drugs or drug combinations that act on distinct disease mechanisms. Since riluzole, which reduces glutamate-induced excitotoxicity (Taketomi and Tsuruta, 2023), remains the most widely used ALS drug, we propose that studying its interactions and potential synergistic effects with new compounds in cellular and preclinical models is a critical step before clinical application. In parallel, identifying progression-related biomarkers, such as specific miRNAs, may support more targeted and adaptive therapeutic strategies.

Our group has focused on developing kinase inhibitors for neurodegenerative diseases, particularly ALS (Seok, 2025). CK1**δ** has been identified as a key regulator of TDP-43 phosphorylation at multiple sites (Loffreda et al., 2020; Paez-Colasante et al., 2020a). Among our

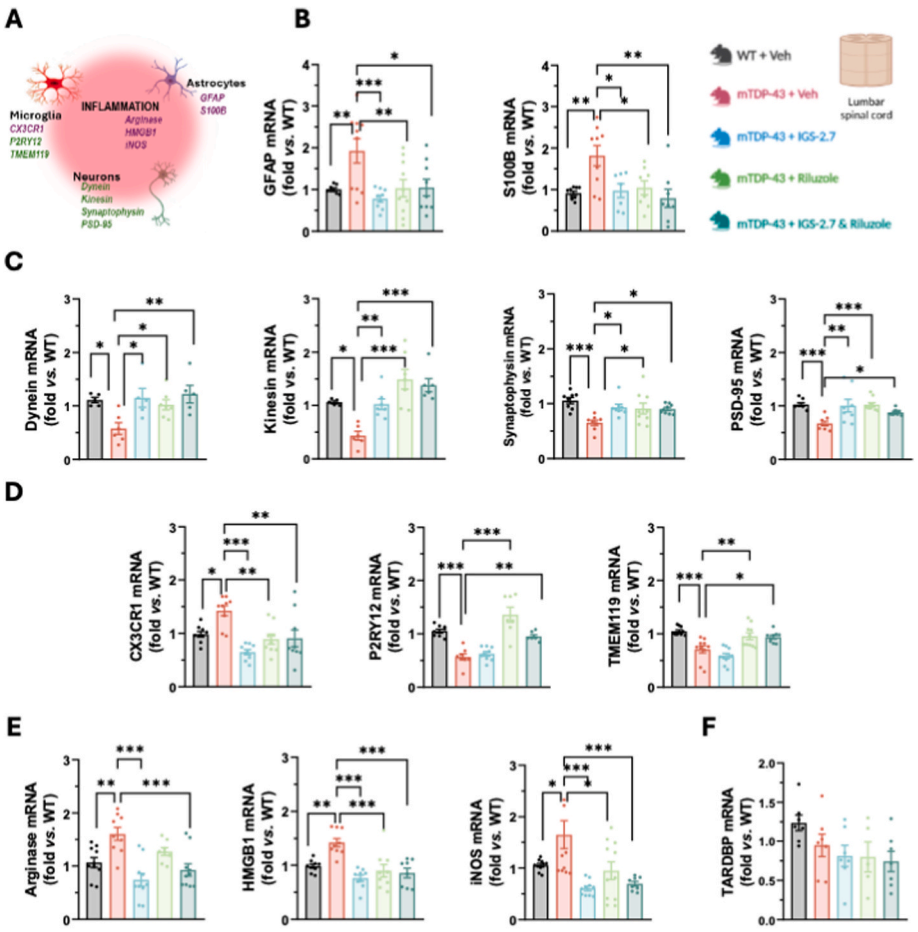

Fig. 7. Identification of neurodegeneration/neuroinflammation-associated genes in the lumbar spinal cord of TDP43(A315T) Tg mice upon 30 days of treatment with vehicle, IGS2.7, riluzole, or their combination. Hybrid C57Bl6/JxCBA mice were used as wild-type (WT) mice control after vehicle administration. Daily intraperitoneal (IP) administrations were initiated at the early symptomatic period (65 days-old) and lasted until the symptomatic stage (95 days-old). Mouse sacrifice was performed 24 h after the last treatment and the spinal cord was collected. A) Schematic representation of neuron-glia upregulated (purple) and downregulated (green) genes in the symptomatic TDP43(A315T) Tg mice as compared with WT, upon vehicle administration. B) Astrocyte-phenotypic genes. C) Neurodegeneration-associated genes. D) Microglia-phenotypic genes. E) Inflammation-associated genes. F) TARDBP mouse gene. ***$p < 0.001$, **$p < 0.01$ and *$p < 0.05$ vs. WT + vehicle. GFAP, glial fibrillary acidic protein; S100B, S100 calcium-binding protein B; PSD-95, postsynaptic density protein-95; CX3CR1, C-X3-C motif chemokine receptor 1; P2RY12 purinergic receptor P2Y, G-coupled, 12; TMEM119, transmembrane protein 119; TARDBP, transactive response DNA binding protein 43 kDa. (For interpretation of the references to colour in this figure legend, the reader is referred to the Web version of this article.)

compounds, IGS2.7, a benzothiazole derivative that selectively inhibits CK1δ, has shown promising results. It reduces TDP-43 phosphorylation and neurotoxicity *in vitro* and in *Drosophila* ALS models (Babazadeh et al., 2023), as well as in human cell models derived from FTLD (Palomo et al., 2021) and ALS patients (Cuevas et al., 2024). Its favourable pharmacokinetic profile led to testing in a TDP-43 transgenic ALS mouse model, where a 1 mg/kg dose significantly protected MN, reduced microglial activation, and decreased spinal TDP-43 phosphorylation (Alquezar et al., 2016).

Building on these findings, we investigated the combined use of IGS2.7 and riluzole in cellular and *in vivo* models to evaluate potential interactions and explore synergistic effects that might enhance therapeutic efficacy beyond monotherapy.

We first employed lymphoblastoid cell lines from sALS patients, which recapitulate key ALS-related features, including TDP-43 proteinopathy (Cuevas et al., 2024). Notably, these cells also exhibited significantly elevated CK1δ mRNA, protein expression, and kinase activity compared to controls. These findings are consistent with previous studies reporting increased CK1δ expression in the frontal cortex and, to a lesser extent, in the spinal cord of sALS patients, reinforcing the utility of these immortalised cells as a model for evaluating CK1**δ** -targeted therapies. We next analysed the combined effect of IGS2.7 and riluzole on TDP-43 homeostasis and protein aggregation in both sALS lymphoblasts and controls. While riluzole alone at subeffective doses had no significant impact on TDP-43 phosphorylation or localization, IGS2.7 alone reduced phosphorylation and restored nuclear localization. Co-treatment further enhanced these effects, particularly in reducing phosphorylation, suggesting a synergistic interaction that may amplify neuroprotective outcomes. This is not without precedent, since similar synergistic effects have been described for other low-dose drug combinations in cellular models (Li et al., 2020).

Cytoplasmic mislocalisation of TDP-43, a hallmark of ALS pathology (Zhou et al., 2018; Pinto et al., 2017), contributes to neuronal dysfunction via loss of nuclear function and protein aggregation. Our immunofluorescence and turbidity assays showed that both IGS2.7 and riluzole partially prevented TDP-43 nuclear export and reduced protein aggregation in sALS lymphoblasts, with the combined treatment producing the most pronounced effects. These findings highlight the synergistic potential of dual therapy targeting CK1δ and glutamate excitotoxicity to restore TDP-43 homeostasis and reduce proteostatic stress.

Given the promising *in vitro* findings, we evaluated the effects of IGS2.7 and riluzole, alone and in combination, in a TDP-43(A315T) Tg ALS mouse model (Brooks et al., 2000). We first confirmed that CK1δ

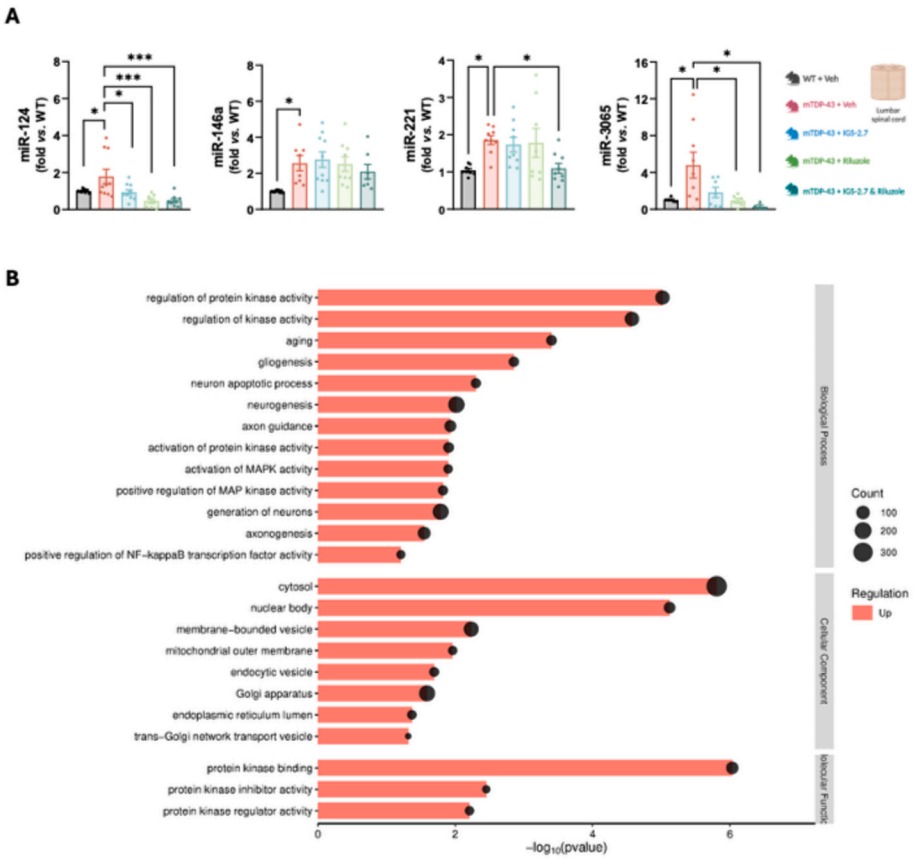

Fig. 8. Profile of dysregulated inflammatory-associated miRNAs in the TDP43 (A315T) Tg mice at the symptomatic stage upon 30 days treatment with vehicle, IGS 2.7, riluzole or their combination. A) miRNA expression evaluated by RT-qPCR; Hybrid C57Bl6/JxCBA mice were used as wild-type (WT) mice control after vehicle administration. ***$p < 0.001$, **$p < 0.01$ and *$p < 0.05$ vs. WT + vehicle. B) Gene ontology (GO) enrichment analysis based on miRNet database (https://www.mirnet.ca/). Functional analysis was classified into biological process (BP), molecular function (MF), and cellular component (CC) in the miRNet platform. Line lengths represent p-value; dot represent gene number (hits).

activity was significantly elevated in both the cerebral cortex and spinal cord of these mice. To assess treatment impact, we conducted two experiments using either effective or subeffective doses. It is worth noting that riluzole has been scarcely evaluated in the TDP-43(A315T) model, and evidence from the SOD1(G93A) model would likely not have justified its clinical development (Han et al., 2023; Ma et al., 2024; Paez-Colasante et al., 2020a; Prasad et al., 2021; Zhou et al., 2019). Moreover, riluzole was approved before validated ALS animal models were available.

In the initial *in vivo* experiment, effective doses of IGS2.7 and riluzole were administered based on previously established protocols in our laboratory (García-Toscano et al., 2025). Co-administration with IGS2.7 resulted in comparable neuroprotective effects on MNs in the dorsal spinal horn and similar reductions in gliosis relative to monotherapy. Notably, no synergistic or adverse effects were observed under the tested conditions, supporting the potential of IGS2.7 as either a stand-alone therapeutic agent or as an adjunct to riluzole.

In the second *in vivo* experiment, we explored whether combining IGS2.7 and riluzole at sub-effective doses could uncover synergistic effects not observed at higher concentrations. Neither treatment alone improved motor performance nor prevented MN loss in TDP-43(A315T) Tg mice, riluzole alone tended to worsen motor outcomes. In contrast, the combined treatment slightly improved motor coordination and significantly preserved MN viability compared to vehicle-treated animals. Although the level of protection did not reach that of WT controls, the findings suggest that therapeutic synergy may emerge at lower doses, potentially allowing for enhanced efficacy with reduced toxicity or potential side effects. These effects were paralleled by the modulation of miR-124-3p, a neuron-enriched microRNA critically involved in maintaining neuro-glial communication. miR-124-3p was markedly upregulated in the spinal cords of symptomatic TDP-43(A315T) Tg mice, in line with previous observations in both animal models and ALS patient samples (Zhou et al., 2018). All treatments, especially the combination, restored miR-124 levels toward baseline. We have previously demonstrated that miR-124-3p is enriched in exosomes from mSOD1 NSC-34 MNs and leads to defective phagocytosis by N9 microglial cells (Pinto et al., 2017). Later, we found that the overexpression of miR-124 in NSC-34 MNs was associated with an increase in early apoptosis, decrease of PSD-95 and kinesin gene expression, as well as changes in mitochondria fusion and fission dynamics, as exhibited by mSOD1 NSC-34 MNs (Vaz et al., 2021). Interestingly, upregulated miR-124-3p was also identified in the spinal cord of SOD1G93A ALS mice at the symptomatic stage, together with activated TLR/NF-kB signaling (Cunha et al., 2018). Moreover, the intrathecal administration of the miR-124-3p inhibitor in the ALS presymptomatic mice prevented the overexpression of miR-124-3p, motor disabilities, gastrocnemius muscle atrophy, neurodegeneration, myelin impairment and immune deregulation at the time of the onset of the disease (Barbosa et al., 2022), revealing to be a promising therapeutic strategy. In conformity, the regulation of miR-124, mainly by IGS2.7 plus riluzole and the

therapeutic benefits we observed in our study reinforces its potential role as both a biomarker and a therapeutic target in ALS, as we show by the predicted mechanisms of action and target prediction. To note that the tested therapeutic strategies, including ISG2.7, are not adversely affecting the *TARDBP* gene's expression.

Regarding glial activation, Iba-1 immunoreactivity revealed no major differences in microglial status across treatment groups, though the combined therapy led to an increase in Iba-1 staining relative to IGS2.7 alone, although the functional significance of this change cannot be determined with the present data. Gene expression analysis showed that vehicle-treated transgenic mice displayed a reactive microglial profile, characterised by elevated Cx3cr1 and suppressed P2ry12 and Tmem119, markers associated with the homeostatic state (Taketomi and Tsuruta, 2023). Some authors suggest that downregulation of *P2ry12* may indicate the down-tuning of microglia intervention in injury-related processes (van Wageningen et al., 2019). Furthermore, low expression of *Tmem119* was also proposed to correspond to a dampened immune response (Ma et al., 2024). All treatments normalized Cx3cr1, while riluzole and the combination therapy partially restored P2ry12 and Tmem119 expression. These changes indicate a partial recovery of microglial homeostasis. In this context, we also assessed miR-146a-5p, a miRNA implicated in feedback regulation of inflammatory signalling via the IRAK1–NF-κB pathway (Zhou et al., 2019). Although it remained elevated across all treatment conditions, the combination therapy showed a slight, non-significant trend toward reduction. Its persistent overexpression may reflect an endogenous compensatory mechanism to restrain excessive cytokine release, as previously suggested in chronic neuroinflammation (Han et al., 2023).

Astrocytic reactivity, a hallmark of ALS pathology, was evident in the TDP-43 model, with increased GFAP immunoreactivity and upregulation of Gfap and S100b transcripts. While histological levels remained elevated following treatment, transcript expression was significantly reduced across all groups, pointing to a regulatory effect at the gene expression level. Moreover, inflammatory mediators Arginase, Hmgb1, and iNOS were also upregulated in the model and were effectively normalized by IGS2.7, either alone or in combination with riluzole. This anti-inflammatory effect was accompanied by the downregulation of miR-3065-5p, recently identified as upregulated in ALS and potentially involved in immune regulation (Paez-Colasante et al., 2020b). Although its specific function is not yet fully characterised, its expression pattern and sensitivity to treatment suggest it may participate in modulating the inflammatory milieu in ALS.

To further explore neuronal integrity, we analysed genes related to axonal transport and synaptic function, both of which are commonly impaired in ALS. Transgenic mice exhibited reduced expression of dynein, kinesin, synaptophysin, and PSD-95, indicating deficits in intracellular trafficking and synaptic maintenance. All treatments led to partial recovery of these markers. Notably, only the combination therapy normalized miR-221-3p, a miRNA involved in stress granule formation (Prasad et al., 2021), RNA-binding protein metabolism, and TDP-43 regulation. Its modulation suggests that the dual therapy not only targets protein aggregation but may also support RNA homeostasis and synaptic resilience, critical components of early neurodegenerative processes.

Altogether, these findings reveal that low-dose co-administration of IGS2.7 and riluzole exerts protective effects across multiple ALS-relevant pathways, including MN survival, glial regulation, synaptic maintenance, and inflammatory control. The coordinated modulation of key miRNAs alongside functional and molecular readouts supports the potential of this multitarget strategy to engage converging mechanisms of ALS pathology and warrants further exploration in long-term and translational models.

5. Conclusion

ALS is a devastating disease with a significant unmet medical need. Riluzole, a glutamate antagonist, remains the only globally approved drug for the treatment of ALS, although it only extends some months of patient survival. Given the urgent need for effective therapies, new chemical entities are also emerging. In particular, the CK1δ inhibitor benzothiazole compound IGS2.7 has shown the ability to functionally restore TDP-43 homeostasis and prevent its cell-to-cell propagation in patient-derived cellular models. In a TDP-43 Tg mouse model, IGS2.7 preserves spinal cord MNs, counteracts microglia dyshomeostasis, and decreases miR-124-3p, miR-221-3p, miR-3065, and phosphorylated TDP-43 levels. While these findings are promising, clinical trials are needed to confirm its therapeutic potential. As riluzole remains the standard of care, it is crucial to evaluate whether combined treatment with IGS2.7 may worsen adverse effects or, conversely, produce synergistic benefits.

Our results, obtained in both patient-derived cellular models and TDP-43(A315T) Tg mice, using a variety of methodologies and endpoints, demonstrate that co-administration of IGS2.7 and riluzole at effective doses does not cause adverse effects. However, no additive benefit was observed over IGS2.7 monotherapy, suggesting that IGS2.7 may be suitable either as a future stand-alone treatment or as an add-on to riluzole.

Interestingly, when sub-optimal doses of both drugs were used, a synergistic effect emerged, improving multiple pathological features of ALS, including nuclear recovery of TDP-43 and preservation of spinal cord MNs. These results suggest that, once IGS2.7 becomes available for clinical testing, its co-administration with a half-dose of riluzole, could potentially enhance therapeutic efficacy while minimizing side effects. Further *in vivo* studies will be important to explore this possibility, although only clinical trials can ultimately confirm its clinical relevance.

CRediT authorship contribution statement

Marta Gomez-Almeria: Methodology, Investigation. **Loreto Martinez-Gonzalez:** Methodology, Investigation. **Ana Teresa Matos:** Methodology, Investigation. **Carmen Rodriguez-Cueto:** Validation, Supervision. **Ana Rita Vaz:** Visualization, Validation, Supervision, Software. **Raquel Martín-Baquero:** Methodology, Investigation. **Carmen Pérez de la Lastra:** Software, Methodology, Investigation. **Rafael Infantes:** Data curation, Methodology. **Javier Fernández-Ruiz:** Writing – review & editing, Formal analysis. **Valle Palomo:** Writing – review & editing, Validation, Supervision, Formal analysis, Conceptualization. **Carmen Gil:** Writing – review & editing, Validation, Resources, Project administration. **Dora Brites:** Writing – review & editing, Writing – original draft, Validation, Project administration, Funding acquisition, Data curation, Conceptualization. **Ana Martinez:** Writing – review & editing, Writing – original draft, Validation, Resources, Project administration, Funding acquisition, Conceptualization. **Eva de Lago:** Writing – review & editing, Writing – original draft, Supervision, Project administration, Investigation, Funding acquisition, Formal analysis, Conceptualization.

Availability of data and materials

Data supporting reported results may be supplied upon request to the authors.

Funding

This work was supported by La Caixa and Luzón Foundations [grant number HR21-00931], the Instituto de Salud Carlos III [CIBERNED, grant numbers CB18/05/00040 and CB06/05/0089], MCINN (PID2021-128906OB-100), and UID/04138/2025 (https://doi.org/10.54499/UID/04138/2025, iMed.ULisboa). VP acknowledges RYC2019-027489-I, funded by MCIN/AEI/10.13039/501100011033 and by El FSE invierte en tu futuro", PID2021-128340OA-I00 funded by MCIN/AEI/10.13039/501100011033 and European Union NextGenerationEU/PRTR. CPL thanks MCIN/AEI/10.13039/501100011033 and FSE "invierte en tu futuro" for her predoctoral funding (PRE2022-102282) within the project PID2021-128340OA-I00.

Declaration of competing interest

The authors declare that they have no known competing financial interests or personal relationships that could have appeared to influence the work reported in this paper.

Appendix A. Supplementary data

Supplementary data to this article can be found online at https://doi.org/10.1016/j.neuropharm.2025.110804.

References

Alquezar, C., Salado, I.G., de la Encarnación, A., Pérez, D.I., Moreno, F., Gil, C., de Munain, A.L., Martínez, A., Martín-Requero, Á., 2016. Targeting TDP-43 phosphorylation by Casein Kinase-1δ inhibitors: a novel strategy for the treatment of frontotemporal dementia. Mol. Neurodegener. 11, 36. https://doi.org/10.1186/s13024-016-0102-7.

Alvarez, F.J., Lafuente, H., Rey-Santano, M.C., Mielgo, V.E., Gastiasoro, E., Rueda, M., Pertwee, R.G., Castillo, A.I., Romero, J., Martínez-Orgado, J., 2008. Neuroprotective effects of the nonpsychoactive cannabinoid cannabidiol in hypoxic-ischemic newborn piglets. Pediatr. Res. 64, 653–658. https://doi.org/10.1203/PDR.0b013e318186e5dd.

Babazadeh, A., Rayner, S.L., Lee, A., Chung, R.S., 2023. TDP-43 as a therapeutic target in neurodegenerative diseases: focusing on motor neuron disease and frontotemporal dementia. Ageing Res. Rev. 92, 102085. https://doi.org/10.1016/j.arr.2023.102085.

Barbosa, M., Gomes, C., Sequeira, C., Gonçalves-Ribeiro, J., Pina, C.C., Carvalho, L.A., Moreira, R., Vaz, S.H., Vaz, A.R., Brites, D., 2021. Recovery of depleted miR-146a in ALS cortical astrocytes reverts cell aberrancies and prevents paracrine pathogenicity on Microglia and motor neurons. Front. Cell Dev. Biol. 9. https://doi.org/10.3389/fcell.2021.634355.

Barbosa, M., Santos, M., de Sousa, N., Duarte-Silva, S., Vaz, A.R., Salgado, A.J., Brites, D., 2022. Intrathecal injection of the secretome from ALS motor neurons regulated for miR-124 expression prevents disease outcomes in SOD1-G93A mice. Biomedicines 10, 2120. https://doi.org/10.3390/biomedicines10092120.

Bensimon, G., Lacomblez, L., Meininger, V., 1994. A controlled trial of riluzole in amyotrophic lateral sclerosis. ALS/Riluzole Study Group. N. Engl. J. Med. 330, 585–591. https://doi.org/10.1056/NEJM199403033300901.

Brooks, B.R., Miller, R.G., Swash, M., Munsat, T.L., 2000. World Federation of neurology research group on motor neuron diseases, El escorial revisited: revised criteria for the diagnosis of amyotrophic lateral sclerosis, amyotroph. Lateral scler. Mot. Neuron Disord. Off. Publ. World Fed. Neurol. Res. Group Mot. Neuron Dis. 1, 293–299. https://doi.org/10.1080/146608200300079536.

Cuevas, E.P., Rodríguez-Fernández, A., Palomo, V., Martínez, A., Martín-Requero, Á., 2022. TDP-43 pathology and prionic behavior in human cellular models of Alzheimer's disease patients. Biomedicines 10, 385. https://doi.org/10.3390/biomedicines10020385.

Cuevas, E.P., Martinez-Gonzalez, L., Gordillo, C., Tosat-Bitrián, C., Pérez de la Lastra, C., Sáenz, A., Gil, C., Palomo, V., Martin-Requero, Á., Martinez, A., 2024. Casein kinase 1 inhibitor avoids TDP-43 pathology propagation in a patient-derived cellular model of amyotrophic lateral sclerosis. Neurobiol. Dis. 192, 106430. https://doi.org/10.1016/j.nbd.2024.106430.

Cunha, C., Santos, C., Gomes, C., Fernandes, A., Correia, A.M., Sebastião, A.M., Vaz, A.R., Brites, D., 2018. Downregulated glia interplay and increased miRNA-155 as promising markers to track ALS at an early stage. Mol. Neurobiol. 55, 4207–4224. https://doi.org/10.1007/s12035-017-0631-2.

Espejo-Porras, F., Piscitelli, F., Verde, R., Ramos, J.A., Di Marzo, V., de Lago, E., Fernández-Ruiz, J., 2015. Changes in the endocannabinoid signaling system in CNS structures of TDP-43 transgenic mice: relevance for a neuroprotective therapy in TDP-43-related disorders. J. Neuroimmune Pharmacol. 10, 233–244. https://doi.org/10.1007/s11481-015-9602-4.

Espejo-Porras, F., García-Toscano, L., Rodríguez-Cueto, C., Santos-García, I., de Lago, E., Fernandez-Ruiz, J., 2019. Targeting glial cannabinoid CB2 receptors to delay the progression of the pathological phenotype in TDP-43 (A315T) transgenic mice, a model of amyotrophic lateral sclerosis. Br. J. Pharmacol. 176, 1585–1600. https://doi.org/10.1111/bph.14216.

Fang, T., Al Khleifat, A., Meurgey, J.-H., Jones, A., Leigh, P.N., Bensimon, G., Al-Chalabi, A., 2018. Stage at which riluzole treatment prolongs survival in patients with amyotrophic lateral sclerosis: a retrospective analysis of data from a dose-ranging study. Lancet Neurol. 17, 416–422. https://doi.org/10.1016/S1474-4422(18)30054-1.

Feldman, E.L., Goutman, S.A., Petri, S., Mazzini, L., Savelieff, M.G., Shaw, P.J., Sobue, G., 2022. Amyotrophic lateral sclerosis. Lancet 400, 1363–1380. https://doi.org/10.1016/S0140-6736(22)01272-7.

García-Toscano, L, Rodríguez-Cueto, C, Furiano, A, Hind, W, de Lago, E, Fernández-Ruiz, J, 2025. Preclinical evaluation of cannabidiolic acid as a neuroprotective agent in TDP-43 transgenic mice, an experimental model of amyotrophic lateral sclerosis. Biomed. Pharmacother. 189, 118288. https://doi.org/10.1016/j.biopha.2025.118288.

Han, R., Gao, J., Wang, L., Hao, P., Chen, X., Wang, Y., Jiang, Z., Jiang, L., Wang, T., Zhu, L., Li, X., 2023. MicroRNA-146a negatively regulates inflammation via the IRAK1/TRAF6/NF-κB signaling pathway in dry eye. Sci. Rep. 13, 11192. https://doi.org/10.1038/s41598-023-38367-4.

Herdewyn, S., Cirillo, C., Van Den Bosch, L., Robberecht, W., Vanden Berghe, P., Van Damme, P., 2014a. Prevention of intestinal obstruction reveals progressive neurodegeneration in mutant TDP-43 (A315T) mice. Mol. Neurodegener. 9, 24. https://doi.org/10.1186/1750-1326-9-24.

Herdewyn, S., Cirillo, C., Van Den Bosch, L., Robberecht, W., Vanden Berghe, P., Van Damme, P., 2014b. Prevention of intestinal obstruction reveals progressive neurodegeneration in mutant TDP-43 (A315T) mice. Mol. Neurodegener. 9, 24. https://doi.org/10.1186/1750-1326-9-24.

Ibarreta, D., Parrilla, R., Ayuso, M.S., 1997. Altered Ca2+ homeostasis in lymphoblasts from patients with late-onset alzheimer disease. Alzheimer Dis. Assoc. Disord. 11, 220–227.

Jaiswal, M.K., 2017. Riluzole but not melatonin ameliorates acute motor neuron degeneration and moderately inhibits SOD1-Mediated excitotoxicity induced disrupted mitochondrial Ca2+ signaling in amyotrophic lateral sclerosis. Front. Cell. Neurosci. 10. https://www.frontiersin.org/articles/10.3389/fncel.2016.00295. (Accessed 28 November 2023).

Krus, K.L., Strickland, A., Yamada, Y., Devault, L., Schmidt, R.E., Bloom, A.J., Milbrandt, J., DiAntonio, A., 2022. Loss of Stathmin-2, a hallmark of TDP-43-associated ALS, causes motor neuropathy. Cell Rep. 39, 111001. https://doi.org/10.1016/j.celrep.2022.111001.

Li, C., Chen, Y., Chen, X., Wei, Q., Ou, R., Gu, X., Cao, B., Shang, H., 2020. MicroRNA-183-5p is stress-inducible and protects neurons against cell death in amyotrophic lateral sclerosis. J. Cell Mol. Med. 24, 8614–8622. https://doi.org/10.1111/jcmm.15490.

Loffreda, A., Nizzardo, M., Arosio, A., Ruepp, M.-D., Calogero, R.A., Volinia, S., Galasso, M., Bendotti, C., Ferrarese, C., Lunetta, C., Rizzuti, M., Ronchi, A.E., Mühlemann, O., Tremolizzo, L., Corti, S., Barabino, S.M.L., 2020. miR-129-5p: a key factor and therapeutic target in amyotrophic lateral sclerosis. Prog. Neurobiol. 190, 101803. https://doi.org/10.1016/j.pneurobio.2020.101803.

Ludolph, A.C., Grandjean, H., Reviers, E., De Micheli, V., Bianchi, C., Cardosi, L., Russ, H., Silani, V., 2023. The preferences of people with amyotrophic lateral sclerosis on riluzole treatment in Europe. Sci. Rep. 13, 22497. https://doi.org/10.1038/s41598-023-49424-3.

Ma, W., Oswald, J., Rios Angulo, A., Chen, Q., 2024. Tmem119 expression is downregulated in a subset of brain metastasis-associated microglia. BMC Neurosci. 25, 6. https://doi.org/10.1186/s12868-024-00846-3.

Martínez-González, L., Rodríguez-Cueto, C., Cabezudo, D., Bartolomé, F., Andrés-Benito, P., Ferrer, I., Gil, C., Martín-Requero, Á., Fernández-Ruiz, J., Martínez, A., de Lago, E., 2020. Motor neuron preservation and decrease of in vivo TDP-43 phosphorylation by protein CK-1δ kinase inhibitor treatment. Sci. Rep. 10, 4449. https://doi.org/10.1038/s41598-020-61265-y.

Mitchell, J.C., McGoldrick, P., Vance, C., Hortobagyi, T., Sreedharan, J., Rogelj, B., Tudor, E.L., Smith, B.N., Klasen, C., Miller, C.C.J., Cooper, J.D., Greensmith, L., Shaw, C.E., 2013. Overexpression of human wild-type FUS causes progressive motor neuron degeneration in an age- and dose-dependent fashion. Acta Neuropathol. 125, 273–288. https://doi.org/10.1007/s00401-012-1043-z.

Paez-Colasante, X., Figueroa-Romero, C., Rumora, A.E., Hur, J., Mendelson, F.E., Hayes, J.M., Backus, C., Taubman, G.F., Heinicke, L., Walter, N.G., Barmada, S.J., Sakowski, S.A., Feldman, E.L., 2020a. Cytoplasmic TDP43 binds microRNAs: new disease targets in amyotrophic lateral sclerosis. Front. Cell. Neurosci. 14, 117. https://doi.org/10.3389/fncel.2020.00117.

Paez-Colasante, X., Figueroa-Romero, C., Rumora, A.E., Hur, J., Mendelson, F.E., Hayes, J.M., Backus, C., Taubman, G.F., Heinicke, L., Walter, N.G., Barmada, S.J., Sakowski, S.A., Feldman, E.L., 2020b. Cytoplasmic TDP43 binds microRNAs: new disease targets in amyotrophic lateral sclerosis. Front. Cell. Neurosci. 14. https://doi.org/10.3389/fncel.2020.00117.

Palomo, V., Nozal, V., Rojas-Prats, E., Gil, C., Martinez, A., 2021. Protein kinase inhibitors for amyotrophic lateral sclerosis therapy. Br. J. Pharmacol. 178, 1316–1335. https://doi.org/10.1111/bph.15221.

Pansarasa, O., Bordoni, M., Drufuca, L., Diamanti, L., Sproviero, D., Trotti, R., Bernuzzi, S., La Salvia, S., Gagliardi, S., Ceroni, M., Cereda, C., 2018. Lymphoblastoid cell lines as a model to understand amyotrophic lateral sclerosis disease mechanisms. Dis. Model. Mech. 11. https://doi.org/10.1242/dmm.031625 dmm031625.

Pegoraro, V., Merico, A., Angelini, C., 2017. Micro-RNAs in ALS muscle: differences in gender, age at onset and disease duration. J. Neurol. Sci. 380, 58–63. https://doi.org/10.1016/j.jns.2017.07.008.

Pérez de la Lastra Aranda, C., Tosat-Bitrián, C., Porras, G., Dafinca, R., Muñoz-Torrero, D., Talbot, K., Martín-Requero, Á., Martínez, A., Palomo, V., 2024. Proteome aggregation in cells derived from amyotrophic lateral sclerosis patients for personalized drug evaluation. ACS Chem. Neurosci. 15, 3945–3953. https://doi.org/10.1021/acschemneuro.4c00328.

Pinto, S., Cunha, C., Barbosa, M., Vaz, A.R., Brites, D., 2017. Exosomes from NSC-34 cells transfected with hSOD1-G93A are enriched in miR-124 and drive alterations in microglia phenotype. Front. Neurosci. 11. https://doi.org/10.3389/fnins.2017.00273.

Posa, D., Martínez-González, L., Bartolomé, F., Nagaraj, S., Porras, G., Martínez, A., Martín-Requero, Á., 2019. Recapitulation of pathological TDP-43 features in immortalized lymphocytes from sporadic ALS patients. Mol. Neurobiol. 56, 2424–2432. https://doi.org/10.1007/s12035-018-1249-8.

Prasad, K., Alasmari, A.F., Ali, N., Khan, R., Alghamdi, A., Kumar, V., 2021. Insights into the SARS-CoV-2-Mediated alteration in the stress granule protein regulatory networks in humans. Pathogens 10, 1459. https://doi.org/10.3390/pathogens10111459.

Rodríguez-Cueto, C., Gómez-Almería, M., García Toscano, L., Romero, J., Hillard, C.J., de Lago, E., Fernández-Ruiz, J., 2021. Inactivation of the CB2 receptor accelerated the neuropathological deterioration in TDP-43 transgenic mice, a model of amyotrophic lateral sclerosis. Brain Pathol. Zurich Switz 31, e12972. https://doi.org/10.1111/bpa.12972.

Saitoh, Y., Takahashi, Y., 2020. Riluzole for the treatment of amyotrophic lateral sclerosis. Neurodegener. Dis. Manag. 10, 343–355. https://doi.org/10.2217/nmt-2020-0033.

Salado, I.G., Redondo, M., Bello, M.L., Perez, C., Liachko, N.F., Kraemer, B.C., Miguel, L., Lecourtois, M., Gil, C., Martinez, A., Perez, D.I., 2014. Protein kinase CK-1 inhibitors as new potential drugs for amyotrophic lateral sclerosis. J. Med. Chem. 57, 2755–2772. https://doi.org/10.1021/jm500065f.

Seok, H.Y., 2025. Critical issues in the use of edaravone for the treatment of amyotrophic lateral sclerosis. Neurol. Sci. Off. J. Ital. Neurol. Soc. Ital. Soc. Clin. Neurophysiol. https://doi.org/10.1007/s10072-025-08154-2.

Shmueli, M.D., Hizkiahou, N., Peled, S., Gazit, E., Segal, D., 2017. Total proteome turbidity assay for tracking global protein aggregation in the natural cellular environment. J. Biol. Method. 4, e69. https://doi.org/10.14440/jbm.2017.148.

Taketomi, T., Tsuruta, F., 2023. Towards an understanding of microglia and border-associated macrophages. Biology 12, 1091. https://doi.org/10.3390/biology12081091.

Vaca, G., Martinez-Gonzalez, L., Fernandez, A., Rojas-Prats, E., Porras, G., Cuevas, E.P., Gil, C., Martinez, A., Martin-Requero, Á., 2021. Therapeutic potential of novel cell division cycle kinase 7 inhibitors on TDP-43-related pathogenesis such as frontotemporal lobar degeneration (FTLD) and amyotrophic lateral sclerosis (ALS). J. Neurochem. 156, 379–390. https://doi.org/10.1111/jnc.15118.

van Wageningen, T.A., Vlaar, E., Kooij, G., Jongenelen, C.A.M., Geurts, J.J.G., van Dam, A.-M., 2019. Regulation of microglial TMEM119 and P2RY12 immunoreactivity in multiple sclerosis white and grey matter lesions is dependent on their inflammatory environment. Acta Neuropathol. Commun. 7, 206. https://doi.org/10.1186/s40478-019-0850-z.

Vaz, A.R., Vizinha, D., Morais, H., Colaço, A.R., Loch-Neckel, G., Barbosa, M., Brites, D., 2021. Overexpression of miR-124 in motor neurons plays a key role in ALS pathological processes. Int. J. Mol. Sci. 22, 6128. https://doi.org/10.3390/ijms22116128.

Wegorzewska, I., Bell, S., Cairns, N.J., Miller, T.M., Baloh, R.H., 2009. TDP-43 mutant transgenic mice develop features of ALS and frontotemporal lobar degeneration. Proc. Natl. Acad. Sci. U. S. A 106, 18809–18814. https://doi.org/10.1073/pnas.0908767106.

Zhou, F., Zhang, C., Guan, Y., Chen, Y., Lu, Q., Jie, L., Gao, H., Du, H., Zhang, H., Liu, Y., Wang, X., 2018. Screening the expression characteristics of several miRNAs in G93A-SOD1 transgenic mouse: altered expression of miRNA-124 is associated with astrocyte differentiation by targeting Sox2 and Sox9. J. Neurochem. 145, 51–67. https://doi.org/10.1111/jnc.14229.

Zhou, C., Zhao, L., Wang, K., Qi, Q., Wang, M., Yang, L., Sun, P., Mu, H., 2019. MicroRNA-146a inhibits NF-κB activation and pro-inflammatory cytokine production by regulating IRAK1 expression in THP-1 cells. Exp. Ther. Med. 18, 3078–3084. https://doi.org/10.3892/etm.2019.7881.